Pion interferometry in Au+Au and Cu+Cu collisions at √sNN=62.4 and 200 GeV

(STAR Collaboration) Abelev, B. I.; ...; Planinić, Mirko; ...; Poljak, Nikola; ...; Zuo, J. X.

Pion interferometry in Au + Au and Cu + Cu collisions at $\sqrt{s_{NN}} = 62.4$ and 200 GeV

B. I. Abelev,[8] M. M. Aggarwal,[30] Z. Ahammed,[47] B. D. Anderson,[18] D. Arkhipkin,[12] G. S. Averichev,[11] J. Balewski,[22] O. Barannikova,[8] L. S. Barnby,[2] J. Baudot,[16] S. Baumgart,[52] D. R. Beavis,[3] R. Bellwied,[50] F. Benedosso,[27] M. J. Betancourt,[22] R. R. Betts,[8] A. Bhasin,[17] A. K. Bhati,[30] H. Bichsel,[49] J. Bielcik,[10] J. Bielcikova,[10] B. Biritz,[6] L. C. Bland,[3] M. Bombara,[2] B. E. Bonner,[36] M. Botje,[27] J. Bouchet,[18] E. Braidot,[27] A. V. Brandin,[25] E. Bruna,[52] S. Bueltmann,[29] T. P. Burton,[2] M. Bystersky,[10] X. Z. Cai,[40] H. Caines,[52] M. Calderón de la Barca Sánchez,[5] O. Catu,[52] D. Cebra,[5] R. Cendejas,[6] M. C. Cervantes,[42] Z. Chajecki,[28] P. Chaloupka,[10] S. Chattopadhyay,[47] H. F. Chen,[38] J. H. Chen,[18] J. Y. Chen,[51] J. Cheng,[44] M. Cherney,[9] A. Chikanian,[52] K. E. Choi,[34] W. Christie,[3] R. F. Clarke,[42] M. J. M. Codrington,[42] R. Corliss,[22] T. M. Cormier,[50] M. R. Cosentino,[37] J. G. Cramer,[49] H. J. Crawford,[4] D. Das,[5] S. Dash,[13] M. Daugherity,[43] L. C. De Silva,[50] T. G. Dedovich,[11] M. DePhillips,[3] A. A. Derevschikov,[32] R. Derradi de Souza,[7] L. Didenko,[3] P. Djawotho,[42] S. M. Dogra,[17] X. Dong,[21] J. L. Drachenberg,[42] J. E. Draper,[5] F. Du,[52] J. C. Dunlop,[3] M. R. Dutta Mazumdar,[47] W. R. Edwards,[21] L. G. Efimov,[11] E. Elhalhuli,[2] M. Elnimr,[50] V. Emelianov,[25] J. Engelage,[4] G. Eppley,[36] B. Erazmus,[41] M. Estienne,[16] L. Eun,[31] P. Fachini,[3] R. Fatemi,[19] J. Fedorisin,[11] A. Feng,[51] P. Filip,[12] E. Finch,[52] V. Fine,[3] Y. Fisyak,[3] C. A. Gagliardi,[42] L. Gaillard,[2] M. S. Ganti,[47] D. R. Gangadharan,[6] E. J. Garcia-Solis,[8] A. Geromitsos,[41] F. Geurts,[36] V. Ghazikhanian,[6] P. Ghosh,[47] Y. N. Gorbunov,[9] A. Gordon,[3] O. Grebenyuk,[21] D. Grosnick,[46] B. Grube,[34] S. M. Guertin,[6] K. S. F. F. Guimaraes,[37] A. Gupta,[17] N. Gupta,[17] W. Guryn,[3] B. Haag,[5] T. J. Hallman,[3] A. Hamed,[42] J. W. Harris,[52] W. He,[15] M. Heinz,[52] S. Heppelmann,[31] B. Hippolyte,[16] A. Hirsch,[33] E. Hjort,[21] A. M. Hoffman,[22] G. W. Hoffmann,[43] D. J. Hofman,[8] R. S. Hollis,[8] H. Z. Huang,[6] T. J. Humanic,[28] G. Igo,[6] A. Iordanova,[8] P. Jacobs,[21] W. W. Jacobs,[15] P. Jakl,[10] C. Jena,[13] F. Jin,[40] C. L. Jones,[22] P. G. Jones,[2] J. Joseph,[18] E. G. Judd,[4] S. Kabana,[41] K. Kajimoto,[43] K. Kang,[44] J. Kapitan,[10] D. Keane,[18] A. Kechechyan,[11] D. Kettler,[49] V. Yu. Khodyrev,[32] D. P. Kikola,[21] J. Kiryluk,[21] A. Kisiel,[28] S. R. Klein,[21] A. G. Knospe,[52] A. Kocoloski,[22] D. D. Koetke,[46] M. Kopytine,[18] W. Korsch,[19] L. Kotchenda,[25] V. Kouchpil,[10] P. Kravtsov,[25] V. I. Kravtsov,[32] K. Krueger,[1] M. Krus,[10] C. Kuhn,[16] L. Kumar,[30] P. Kurnadi,[6] M. A. C. Lamont,[3] J. M. Landgraf,[3] S. LaPointe,[50] J. Lauret,[3] A. Lebedev,[3] R. Lednicky,[12] C.-H. Lee,[34] J. H. Lee,[3] W. Leight,[22] M. J. LeVine,[3] N. Li,[51] C. Li,[38] Y. Li,[44] G. Lin,[52] S. J. Lindenbaum,[26] M. A. Lisa,[28] F. Liu,[51] J. Liu,[36] L. Liu,[51] T. Ljubicic,[3] W. J. Llope,[36] R. S. Longacre,[3] W. A. Love,[3] Y. Lu,[38] T. Ludlam,[3] G. L. Ma,[40] Y. G. Ma,[40] D. P. Mahapatra,[13] R. Majka,[52] O. I. Mall,[5] L. K. Mangotra,[17] R. Manweiler,[46] S. Margetis,[18] C. Markert,[43] H. S. Matis,[21] Yu. A. Matulenko,[32] T. S. McShane,[9] A. Meschanin,[32] R. Milner,[22] N. G. Minaev,[32] S. Mioduszewski,[42] A. Mischke,[27] J. Mitchell,[36] B. Mohanty,[47] D. A. Morozov,[32] M. G. Munhoz,[37] B. K. Nandi,[14] C. Nattrass,[52] T. K. Nayak,[47] J. M. Nelson,[2] P. K. Netrakanti,[33] M. J. Ng,[4] L. V. Nogach,[32] S. B. Nurushev,[32] G. Odyniec,[21] A. Ogawa,[3] H. Okada,[3] V. Okorokov,[25] D. Olson,[21] M. Pachr,[10] B. S. Page,[15] S. K. Pal,[47] Y. Pandit,[18] Y. Panebratsev,[11] S. Y. Panitkin,[3] T. Pawlak,[48] T. Peitzmann,[27] V. Perevoztchikov,[3] C. Perkins,[4] W. Peryt,[48] S. C. Phatak,[13] M. Planinic,[53] J. Pluta,[48] N. Poljak,[53] A. M. Poskanzer,[21] B. V. K. S. Potukuchi,[17] D. Prindle,[49] C. Pruneau,[50] N. K. Pruthi,[30] J. Putschke,[52] R. Raniwala,[35] S. Raniwala,[35] R. L. Ray,[43] R. Redwine,[22] R. Reed,[5] A. Ridiger,[25] H. G. Ritter,[21] J. B. Roberts,[36] O. V. Rogachevskiy,[11] J. L. Romero,[5] A. Rose,[21] C. Roy,[41] L. Ruan,[3] M. J. Russcher,[27] R. Sahoo,[41] I. Sakrejda,[21] T. Sakuma,[22] S. Salur,[21] J. Sandweiss,[52] M. Sarsour,[42] J. Schambach,[43] R. P. Scharenberg,[33] N. Schmitz,[23] J. Seger,[9] I. Selyuzhenkov,[15] P. Seyboth,[23] A. Shabetai,[16] E. Shahaliev,[11] M. Shao,[38] M. Sharma,[50] S. S. Shi,[51] X.-H. Shi,[40] E. P. Sichtermann,[21] F. Simon,[23] R. N. Singaraju,[47] M. J. Skoby,[33] N. Smirnov,[52] R. Snellings,[27] P. Sorensen,[3] J. Sowinski,[15] H. M. Spinka,[1] B. Srivastava,[33] A. Stadnik,[11] T. D. S. Stanislaus,[46] D. Staszak,[6] M. Strikhanov,[25] B. Stringfellow,[33] A. A. P. Suaide,[37] M. C. Suarez,[8] N. L. Subba,[18] M. Sumbera,[10] X. M. Sun,[21] Y. Sun,[38] Z. Sun,[20] B. Surrow,[22] T. J. M. Symons,[21] A. Szanto de Toledo,[37] J. Takahashi,[7] A. H. Tang,[3] Z. Tang,[38] T. Tarnowsky,[33] D. Thein,[43] J. H. Thomas,[21] J. Tian,[40] A. R. Timmins,[2] S. Timoshenko,[25] D. Tlusty,[10] M. Tokarev,[11] T. A. Trainor,[49] V. N. Tram,[21] A. L. Trattner,[4] S. Trentalange,[6] R. E. Tribble,[42] O. D. Tsai,[6] J. Ulery,[33] T. Ullrich,[3] D. G. Underwood,[1] G. Van Buren,[3] M. van Leeuwen,[27] A. M. Vander Molen,[24] J. A. Vanfossen, Jr.,[18] R. Varma,[14] G. M. S. Vasconcelos,[7] I. M. Vasilevski,[12] A. N. Vasiliev,[32] F. Videbaek,[3] S. E. Vigdor,[15] Y. P. Viyogi,[13] S. Vokal,[11] S. A. Voloshin,[50] M. Wada,[43] W. T. Waggoner,[9] M. Walker,[22] F. Wang,[33] G. Wang,[6] J. S. Wang,[20] Q. Wang,[33] X. Wang,[44] X. L. Wang,[38] Y. Wang,[44] G. Webb,[19] J. C. Webb,[46] G. D. Westfall,[24] C. Whitten, Jr.,[6] H. Wieman,[21] S. W. Wissink,[15] R. Witt,[45] Y. Wu,[51] W. Xie,[33] N. Xu,[21] Q. H. Xu,[39] Y. Xu,[38] Z. Xu,[3] Y. Yang,[20] P. Yepes,[36] I.-K. Yoo,[34] Q. Yue,[44] M. Zawisza,[48] H. Zbroszczyk,[48] W. Zhan,[20] S. Zhang,[40] W. M. Zhang,[18] X. P. Zhang,[21] Y. Zhang,[21] Z. P. Zhang,[38] Y. Zhao,[38] C. Zhong,[40] J. Zhou,[36] R. Zoulkarneev,[12] Y. Zoulkarneeva,[12] and J. X. Zuo[40]

(STAR Collaboration)

[1]*Argonne National Laboratory, Argonne, Illinois 60439, USA*
[2]*University of Birmingham, Birmingham, United Kingdom*
[3]*Brookhaven National Laboratory, Upton, New York 11973, USA*
[4]*University of California, Berkeley, California 94720, USA*
[5]*University of California, Davis, California 95616, USA*
[6]*University of California, Los Angeles, California 90095, USA*
[7]*Universidade Estadual de Campinas, Sao Paulo, Brazil*
[8]*University of Illinois at Chicago, Chicago, Illinois 60607, USA*
[9]*Creighton University, Omaha, Nebraska 68178, USA*

[10]*Nuclear Physics Institute AS CR, 250 68 Řež/Prague, Czech Republic*
[11]*Laboratory for High Energy (JINR), Dubna, Russia*
[12]*Particle Physics Laboratory (JINR), Dubna, Russia*
[13]*Institute of Physics, Bhubaneswar 751005, India*
[14]*Indian Institute of Technology, Mumbai, India*
[15]*Indiana University, Bloomington, Indiana 47408, USA*
[16]*Institut de Recherches Subatomiques, Strasbourg, France*
[17]*University of Jammu, Jammu 180001, India*
[18]*Kent State University, Kent, Ohio 44242, USA*
[19]*University of Kentucky, Lexington, Kentucky 40506-0055, USA*
[20]*Institute of Modern Physics, Lanzhou, People's Republic of China*
[21]*Lawrence Berkeley National Laboratory, Berkeley, California 94720, USA*
[22]*Massachusetts Institute of Technology, Cambridge, Massachusetts 02139-4307, USA*
[23]*Max-Planck-Institut für Physik, Munich, Germany*
[24]*Michigan State University, East Lansing, Michigan 48824, USA*
[25]*Moscow Engineering Physics Institute, Moscow, Russia*
[26]*City College of New York, New York City, New York 10031, USA*
[27]*NIKHEF and Utrecht University, Amsterdam, The Netherlands*
[28]*Ohio State University, Columbus, Ohio 43210, USA*
[29]*Old Dominion University, Norfolk, Virginia 23529, USA*
[30]*Panjab University, Chandigarh 160014, India*
[31]*Pennsylvania State University, University Park, Pennsylvania 16802, USA*
[32]*Institute of High Energy Physics, Protvino, Russia*
[33]*Purdue University, West Lafayette, Indiana 47907, USA*
[34]*Pusan National University, Pusan, Republic of Korea*
[35]*University of Rajasthan, Jaipur 302004, India*
[36]*Rice University, Houston, Texas 77251, USA*
[37]*Universidade de Sao Paulo, Sao Paulo, Brazil*
[38]*University of Science & Technology of China, Hefei 230026, People's Republic of China*
[39]*Shandong University, Jinan, Shandong 250100, People's Republic of China*
[40]*Shanghai Institute of Applied Physics, Shanghai 201800, People's Republic of China*
[41]*SUBATECH, Nantes, France*
[42]*Texas A&M University, College Station, Texas 77843, USA*
[43]*University of Texas, Austin, Texas 78712, USA*
[44]*Tsinghua University, Beijing 100084, People's Republic of China*
[45]*United States Naval Academy, Annapolis, Maryland 21402, USA*
[46]*Valparaiso University, Valparaiso, Indiana 46383, USA*
[47]*Variable Energy Cyclotron Centre, Kolkata 700064, India*
[48]*Warsaw University of Technology, Warsaw, Poland*
[49]*University of Washington, Seattle, Washington 98195, USA*
[50]*Wayne State University, Detroit, Michigan 48201, USA*
[51]*Institute of Particle Physics, CCNU (HZNU), Wuhan 430079, People's Republic of China*
[52]*Yale University, New Haven, Connecticut 06520, USA*
[53]*University of Zagreb, Zagreb, HR-10002, Croatia*

(Received 6 March 2009; published 24 August 2009)

We present a systematic analysis of two-pion interferometry in Au + Au collisions at $\sqrt{s_{NN}} = 62.4$ GeV and Cu + Cu collisions at $\sqrt{s_{NN}} = 62.4$ and 200 GeV using the STAR detector at the Relativistic Heavy Ion Collider (RHIC). The multiplicity and transverse momentum dependences of the extracted correlation lengths (radii) are studied. The scaling with charged particle multiplicity of the apparent system volume at final interaction is studied for the RHIC energy domain. The multiplicity scaling of the measured correlation radii is found to be independent of colliding system and collision energy.

DOI: 10.1103/PhysRevC.80.024905 PACS number(s): 25.75.Nq, 25.75.Gz

I. INTRODUCTION

One of the definitive predictions of quantum chromodynamics (QCD) is that at sufficiently high temperature or density [1] strongly interacting matter will be in a state with colored degrees of freedom, i.e., quarks and gluons. The central goal of the experiments with relativistic heavy-ion collisions is to create and study this hypothesized form of matter, called

the quark-gluon plasma (QGP), which might have existed in the microsecond old universe. Numerous experimental observables have been proposed as signatures of QGP creation in heavy-ion collisions [2]. One of these predictions is based on the expectation that the increased number of degrees of freedom associated with the color deconfined state increases the entropy of the system that should survive subsequent hadronization and freeze-out (final interactions). The increased entropy is expected to lead to an increased spatial extent and duration of particle emission, thus providing a significant probe for the QGP phase transition [3,4].

The information about the space-time structure of the emitting source can be extracted with intensity interferometry techniques [5]. This method, popularly known as Hanbury-Brown and Twiss (HBT) correlations, was originally developed to measure angular sizes of stars [6]. The momentum correlations of the produced particles from hadronic sources, however, include dynamical as well as interference effects, hence the term *femtoscopy* [7] is more appropriate. The primary goal of femtoscopy, performed at midrapidity and low transverse momentum, is to study the space-time size of the emitting source and freeze-out processes of the dynamically evolving collision system. Femtoscopic correlations have been successfully studied in most of the heavy-ion experiments (see Ref. [8] for a recent review).

Experimentally, the two-particle correlation function is the ratio,

$$C(\vec{q}, \vec{K}) = \frac{A(\vec{q}, \vec{K})}{B(\vec{q}, \vec{K})}, \tag{1}$$

where $A(\vec{q}, \vec{K})$ is the distribution of pairs of particles with relative momentum $\vec{q} = \vec{p}_1 - \vec{p}_2$ and average momentum $\vec{K} = (\vec{p}_1 + \vec{p}_2)/2$ from the same event and $B(\vec{q}, \vec{K})$ is the corresponding distribution for pairs of particles taken from different events [9,10]. The correlation function is normalized to unity at large $\vec{q}$. With the availability of high statistics data and development of new techniques, it has become possible to measure three-dimensional decompositions of $\vec{q}$ [11–13], providing better insight into the collision geometry.

Previous femtoscopic measurements at the Relativistic Heavy Ion Collider (RHIC) in Au + Au collisions at $\sqrt{s_{NN}} =$ 130 GeV [14,15] and 200 GeV [16,17] obtained qualitatively similar source sizes. However, detailed comparisons with smaller colliding systems and energies are required to understand the dynamics of the source during freeze-out. The crucial information provided from such femtoscopic studies with pions will help to improve our understanding of the reaction mechanisms and to constrain theoretical models of heavy-ion collisions [18–25].

In this article we present a systematic analysis of two-pion interferometry in Au + Au collisions at $\sqrt{s_{NN}} = 62.4$ GeV and Cu + Cu collisions at $\sqrt{s_{NN}} = 62.4$ GeV and 200 GeV using the Solenoidal Tracker at RHIC (STAR) detector. The article is organized as follows: Sec. II explains the detector setup, along with the necessary event, particle, and pair cuts. In Sec. III, the analysis and construction of the correlation function is discussed. The presented results are compared with previous STAR measurements for Au + Au collisions at $\sqrt{s_{NN}} = 200$ GeV in Sec. IV. This section also includes a compilation of freeze-out volume estimates for all available heavy-ion results from Alternating Gradient Synchrotron (AGS), Super Proton Synchrotron (SPS), and RHIC. Section V contains a summary and conclusions.

II. EXPERIMENTAL SETUP, EVENT AND PARTICLE SELECTION

A. The STAR detector and trigger details

The STAR detector [26], which has a large acceptance and is azimuthally symmetric, consists of several detector subsystems and a solenoidal magnet. In the present study the central time projection chamber (TPC) [27] provided the main information used for track reconstruction. It is 4.2 m long and 4 m in diameter. The TPC covers the pseudorapidity region $|\eta| < 1.8$ with full azimuthal coverage ($-\pi < \phi < \pi$). It is a gas chamber filled with P10 gas (10% methane, 90% argon) with inner and outer radii of 50 and 200 cm, respectively, in a uniform electric field of ∼135 V/cm. The paths of the particles passing through the gas are reconstructed from the release of secondary electrons that drift to the readout end caps at both ends of the chamber. The readout system is based on multiwire proportional chambers with cathode pads. There are 45 pad-rows between the inner and outer radii of the TPC.

A minimum bias trigger is obtained using the charged particle hits from an array of scintillator slats arranged in a barrel, called the central trigger barrel, surrounding the TPC, two zero-degree calorimeters (ZDCs) [28] at ±18 m from the detector center along the beam line, and two beam-beam counters. The ZDCs measure neutrons at beam rapidity that originate from the breakup of the colliding nuclei. The centrality determination that is used in this analysis is the uncorrected multiplicity of charged particles in the pseudorapidity region $|\eta| < 0.5$ ($N_{\rm ch}^{\rm TPC}$) as measured by the TPC.

B. Event and centrality selection

For this analysis we selected events with a collision vertex within ±30 cm measured along the beam axis from the center of the TPC. This event selection is applied to all the data sets discussed here.

The events are further binned according to collision centrality that is determined by the measured charged hadron multiplicity within the pseudorapidity range $|\eta| < 0.5$. In Table I we list the centrality bins for Au + Au at $\sqrt{s_{NN}} =$ 62.4 GeV along with the multiplicity bin definitions, average number of participating nucleons and average number of binary nucleon-nucleon collisions [29,30]. For the present analysis we chose six centrality bins corresponding to 0–5%, 5–10%, 10–20%, 20–30%, 30–50%, 50–80% of the total inelastic nucleus-nucleus hadronic cross section. A data set of 2 million minimum-bias trigger events that passed the event cuts is used in the analysis.

TABLE I. Collision centrality selection in terms of percentage of total Au-Au inelastic cross section, number tracks in TPC, average number of participating nucleons, and average number of binary nucleon-nucleon collisions for Au + Au at $\sqrt{s_{NN}} =$ 62.4 GeV.

% cross section	$N_{\rm ch}^{\rm TPC}$	$\langle N_{\rm part}\rangle$	$\langle N_{\rm coll}\rangle$
0–5	>373	$347.3^{+4.3}_{-3.7}$	$904^{+67.7}_{-62.4}$
5–10	372–313	$293.3^{+7.3}_{-5.6}$	$713.7^{+63.7}_{-54.8}$
10–20	312–222	$229.0^{+9.2}_{-7.7}$	$511.8^{+54.9}_{-48.2}$
20–30	221–154	$162.0^{+10.0}_{-9.5}$	$320.9^{+43.0}_{-39.2}$
30–40	153–102	$112.0^{+9.6}_{-9.1}$	$193.5^{+30.4}_{-31.4}$
40–50	101–65	$74.2^{+9.0}_{-8.5}$	$109.3^{+22.1}_{-21.8}$
50–60	64–38	$45.8^{+7.0}_{-7.1}$	$56.6^{+15.0}_{-14.3}$
60–70	37–20	$25.9^{+5.6}_{-5.6}$	$26.8^{+8.8}_{-9.0}$
70–80	19–9	$13.0^{+3.4}_{-4.6}$	$11.2^{+3.7}_{-4.8}$

Tables II and III list the six centrality bins for Cu + Cu at $\sqrt{s_{NN}} = 200$ GeV and 62.4 GeV corresponding to 0–10%, 10–20%, 20–30%, 30–40%, 40–50%, 50–60% of the total hadronic cross section. The number of events used is 15 million and 24 million for 62.4 and 200 GeV Cu + Cu datasets, respectively, after the event cuts.

C. Particle selection

We selected particle tracks in the rapidity region $|y| < 0.5$. Particle identification was performed by correlating the specific ionization of particles in the TPC gas with their measured momenta. For this analysis pions are selected by requiring the specific ionization to be within 2 standard deviations from their theoretical Bichsel value [31,32]. To remove the kaons and protons that could satisfy this condition, particles are also required to be more than 2 standard deviations from the Bichsel value for kaons and protons. Charged particle tracks reconstructed and used for this analysis are accepted if they have space points on at least 15 pad rows in TPC. Tracks with fewer space points may be broken track fragments. These cuts are similar to those in our previous analysis of Au + Au collisions at $\sqrt{s_{NN}} = 200$ GeV [17] because the detector setup was identical.

TABLE II. Collision centrality selection in terms of percentage of total Cu-Cu inelastic cross section, number tracks in TPC, average number of participating nucleons and average number of binary nucleon-nucleon collisions for Cu + Cu at $\sqrt{s_{NN}} =$ 200 GeV.

% cross section	$N_{\rm ch}^{\rm TPC}$	$\langle N_{\rm part}\rangle$	$\langle N_{\rm coll}\rangle$
0–10	>139	$99.0^{+1.5}_{-1.2}$	$188.8^{+15.4}_{-13.4}$
10–20	138–98	$74.6^{+1.3}_{-1.0}$	$123.6^{+9.4}_{-8.3}$
20–30	97–67	$53.7^{+0.9}_{-0.7}$	$77.6^{+5.4}_{-4.7}$
30–40	66–46	$37.8^{+0.7}_{-0.5}$	$47.7^{+2.8}_{-2.7}$
40–50	45–30	$26.2^{+0.5}_{-0.4}$	$29.2^{+1.6}_{-1.4}$
50–60	29–19	$17.2^{+0.4}_{-0.2}$	$16.8^{+0.7}_{-0.7}$

TABLE III. Collision centrality selection in terms of percentage of total Cu-Cu inelastic cross section, number tracks in TPC, average number of participating nucleons, and average number of binary nucleon-nucleon collisions for Cu + Cu at $\sqrt{s_{NN}} =$ 62.4 GeV.

% cross section	$N_{\rm ch}^{\rm TPC}$	$\langle N_{\rm part}\rangle$	$\langle N_{\rm coll}\rangle$
0–10	>101	$96.4^{+1.1}_{-2.6}$	$161.8^{+12.1}_{-13.5}$
10–20	100–71	$72.1^{+0.6}_{-1.9}$	$107.5^{+6.3}_{-8.6}$
20–30	70–49	$51.8^{+0.5}_{-1.2}$	$68.4^{+3.6}_{-4.7}$
30–40	48–33	$36.2^{+0.4}_{-0.8}$	$42.3^{+1.9}_{-2.6}$
40–50	32–22	$24.9^{+0.4}_{-0.6}$	$25.9^{+1.0}_{-1.5}$
50–60	21–14	$16.3^{+0.4}_{-0.3}$	$15.1^{+0.6}_{-0.6}$

D. Pair cuts

Two types of particle track reconstruction errors directly affect measured particle pair densities at the small relative momentum values studied here. Track splitting, in which one particle trajectory is reconstructed as two or more "particles," increases the apparent number of pairs at low relative q. To address this problem we developed a split track filter algorithm, described in our previous analysis of Au + Au collisions at $\sqrt{s_{NN}} = 200$ GeV [17], where values of the splitting level parameter from −0.5 to 0.6 [17] ensured valid tracks. The inefficiencies arising due to track merging, in which two or more particle trajectories are reconstructed as one track, was completely eliminated by requiring that the fraction of merged hits (overlapping space-charge depositions in the TPC gas) be less than 10% for every track pair used in the correlation function.

In the present analysis, we used the same cuts to remove splitting and merging as were used for Au + Au collisions at $\sqrt{s_{NN}} = 200$ GeV [17]. The track pairs are required to have an average transverse momentum $[k_T = (|\vec{p}_{1T} + \vec{p}_{2T}|)/2]$ in one of four bins corresponding to [150,250] MeV/c, [250, 350] MeV/c, [350,450] MeV/c, and [450,600] MeV/c. The results are presented and discussed as a function of k_T and m_T $(=\sqrt{k_T^2 + m_\pi^2})$ in each of those bins.

III. ANALYSIS METHOD

A. Correlation function

The numerator and denominator of the two-particle correlation function in Eq. (1) are constructed by filling histograms corresponding to particle pairs from the same event and from mixed events, respectively. The background pairs are constructed from mixed events [9] where by pairing each particle in a given event is mixed with all particles from other events within a subset of 10 similar events. The events for mixing are selected within the given centrality bin such that

their respective primary vertex z positions are all within 10 cm of one another.

B. Bertsch-Pratt parametrizations and Coulomb interactions

We decompose the relative momentum $\vec{q}$ according to the Bertsch-Pratt (or "out-side-long") convention [11–13,33,34]. The relative momentum $\vec{q}$ is decomposed into the variables $q_{\rm long}$ along the beam direction, $q_{\rm out}$ parallel to the transverse momentum of the pair $\vec{k}_{\rm T} = (\vec{p}_{1\rm T} + \vec{p}_{2\rm T})/2$, and $q_{\rm side}$ perpendicular to $q_{\rm long}$ and $q_{\rm out}$.

In addition to the correlation arising from the quantum statistics of two identical (boson) particles, correlations can also arise from two-particle final-state interactions even for nonidentical particles [35–37]. For identical pions the effects of strong interactions are negligible, but the long-range Coulomb repulsion causes a suppression of the measured correlation function at small $\vec{q}$.

In this article we follow the procedure used in our previous analysis of Au + Au collisions at $\sqrt{s_{NN}} = 200$ GeV [17]. For an azimuthally integrated analysis at midrapidity in the longitudinal comoving system (LCMS) the correlation function in Eq. (1) can be decomposed as [8,38]:

$$C(q_{\rm out}, q_{\rm side}, q_{\rm long}) = (1-\lambda) + \lambda K_{\rm coul}(q_{\rm inv}) \times \left(1 + e^{-q_{\rm out}^2 R_{\rm out}^2 - q_{\rm side}^2 R_{\rm side}^2 - q_{\rm long}^2 R_{\rm long}^2}\right), \quad (2)$$

where $K_{\rm coul}$ is, to a good approximation, the squared nonsymmetrized Coulomb wave function integrated over a Gaussian source (corresponding to the LCMS Gaussian radii $R_{\rm out}$, $R_{\rm side}$, $R_{\rm long}$). Assuming perfect experimental particle identification and a purely chaotic (incoherent) source, λ represents the fraction of correlated pairs [39].

We assumed a spherical Gaussian source of 5 fm for Au + Au collisions at $\sqrt{s_{NN}} = 62.4$ GeV and a 3 fm source for Cu + Cu collisions at $\sqrt{s_{NN}} = 62.4$ and 200 GeV. The first term $(1-\lambda)$ in Eq. (2) accounts for those pairs that do not interact or interfere and the second term represents those pairs where both Bose-Einstein effects and Coulomb interactions are present [17].

C. Systematic uncertainties

We studied several sources of systematic errors similar to a previously published STAR pion interferometry analysis for Au + Au collisions at $\sqrt{s_{NN}} = 200$ GeV [17]. The following effects are considered: track merging, track splitting, source size assumed for the Coulomb correction, particle identification purity, and particle pair acceptance effects for unlike-sign charged pions. The estimated systematic errors are less than 10% for $R_{\rm out}$, $R_{\rm side}$, $R_{\rm long}$, λ in all centrality and k_T bins for the present data sets and are similar to those in Ref. [17]. This similarity is expected because the detector setup was identical and similar particle and pair selection cuts are used for Au + Au and Cu + Cu collisions. Results shown in the figures for the present data sets include statistical errors only.

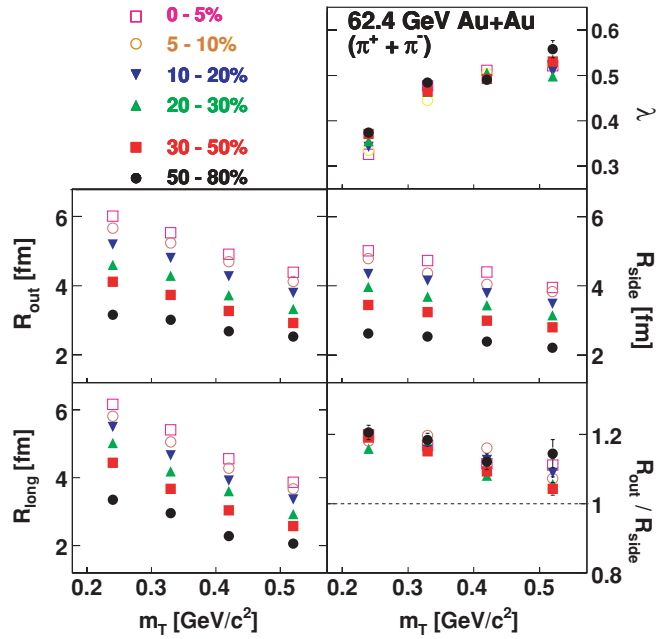

FIG. 1. (Color online) The femtoscopic parameters vs. m_T for six different centralities for Au + Au collisions at $\sqrt{s_{NN}} = 62.4$ GeV. Only statistical errors are shown. The estimated systematic errors are less than 10% for $R_{\rm out}$, $R_{\rm side}$, $R_{\rm long}$, λ in all centrality and k_T bins.

IV. RESULTS AND DISCUSSION

A. Au + Au collisions at $\sqrt{s_{NN}} = 62.4$ GeV

The correlation function in Eq. (2) is fitted to the 3D correlation data for Au + Au collisions at $\sqrt{s_{NN}} = 62.4$ GeV for each centrality and m_T bins as defined above. The analysis is performed separately for $\pi^+\pi^+$ and $\pi^-\pi^-$ pairs. The final histograms for the like-sign pairs do not show appreciable differences and may therefore be summed to increase statistics. Figure 1 presents the results for $R_{\rm out}$, $R_{\rm side}$, $R_{\rm long}$, λ and the ratio, $R_{\rm out}/R_{\rm side}$. The three femtoscopic radii increase with increasing centrality as expected, whereas the values of λ and the $R_{\rm out}/R_{\rm side}$ ratio exhibit no clear centrality dependences.

We observe that for all centralities the three femtoscopic radii decrease with increasing m_T, whereas the λ parameter increases with m_T. Such behavior is consistent with our previous measurements at $\sqrt{s_{NN}} = 200$ GeV [17]. The increase of parameter λ with m_T is due to the decreasing contribution of pions produced from long-lived resonance decays at higher transverse momenta. For comparison, in Fig. 2 we show the results for Au + Au collisions at $\sqrt{s_{NN}} = 62.4$ GeV and 200 GeV for the most central collisions. We observe that the $R_{\rm out}$ values are similar for both cases, but there are differences between the values of $R_{\rm side}$ and $R_{\rm long}$. The $R_{\rm out}/R_{\rm side}$ ratio decreases with increasing m_T, but the values are higher for $\sqrt{s_{NN}} = 62.4$ GeV than for $\sqrt{s_{NN}} = 200$ GeV.

The observed dependences of the three femtoscopic radii are qualitatively consistent with models with collective flow [40–42]. Collective expansion results in position-momentum correlations in both transverse and longitudinal directions. In an expanding source the correlation between the space-time points where the pions are emitted and their energy-momentum

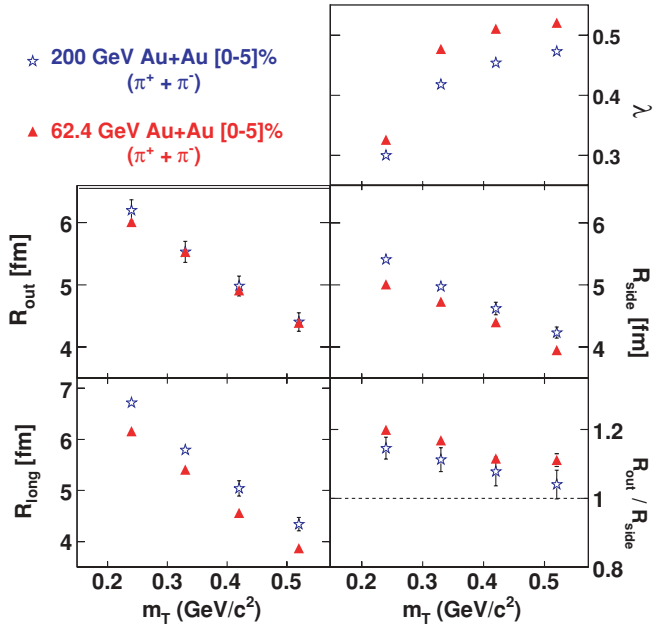

FIG. 2. (Color online) The comparison of femtoscopic measurements of Au + Au collisions at $\sqrt{s_{NN}} = 200$ GeV and 62.4 GeV for 0–5% most central events. Only statistical errors are shown for Au + Au collisions at $\sqrt{s_{NN}} = 62.4$ GeV. The estimated systematic errors for Au + Au collisions at $\sqrt{s_{NN}} = 62.4$ GeV are less than 10% for $R_{\rm out}$, $R_{\rm side}$, $R_{\rm long}$, λ in 0–5% most central events and all k_T bins. The 200 GeV results are from Ref. [17].

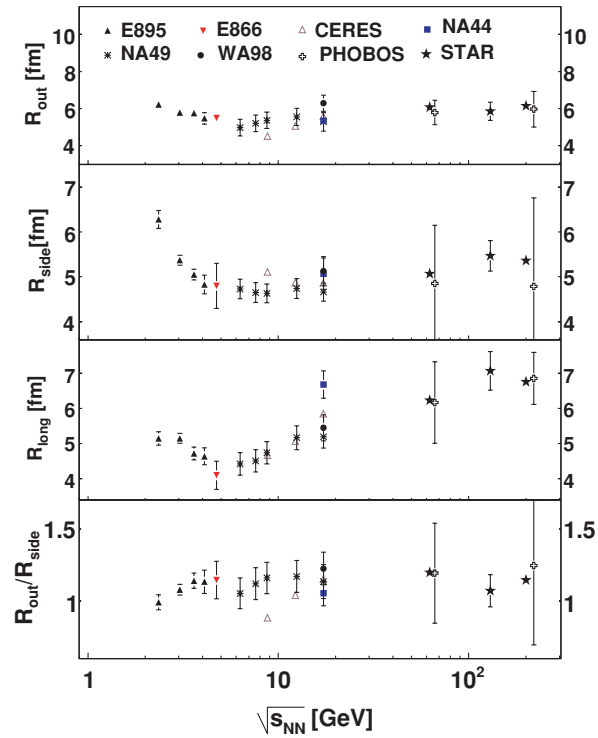

FIG. 3. (Color online) The energy dependence of femtoscopic parameters for AGS, SPS, and RHIC from Refs. [14,17,50–57]. Energy dependences of pion femtoscopic parameters for central Au + Au, Pb + Pb, and Pb + Au collisions are shown for midrapidity and $\langle k_T \rangle \sim 0.2$–$0.3$ GeV/c. Error bars on NA44, NA49, CERES, PHOBOS, and STAR results at $\sqrt{s_{NN}} = 130$ and 200 GeV include systematic uncertainties; error bars on other results are statistical only. Only statistical errors are shown for Au + Au collisions at $\sqrt{s_{NN}} = 62.4$ GeV; the estimated systematic errors are less than 10% for $R_{\rm out}$, $R_{\rm side}$, $R_{\rm long}$. The PHOBOS results from Ref. [50] for $\sqrt{s_{NN}} = 62.4$ and 200 GeV are slightly shifted horizontally for visual clarity.

produce a characteristic dependence of femtoscopic radii on m_T [8,12,22,43–48]. The decrease in the "out" and "side" components can be described by models including transverse flow [17,22,43,45], and the decrease in the "long" component by those with longitudinal flow [17,44,45,49].

B. Energy dependence of femtoscopic radii

In Fig. 3 we present the energy dependences of the three femtoscopic radii and the ratio $R_{\rm out}/R_{\rm side}$ for the available data from AGS, SPS and RHIC. The results are compiled for Au + Au, Pb + Pb, and Pb + Au collisions at midrapidity and for $\langle k_T \rangle \sim 0.2$–$0.3$ GeV/c. The present measurements for Au + Au collisions at $\sqrt{s_{NN}} = 62.4$ GeV are also included. The quality of the present STAR data with respect to statistical and systematic errors is significantly better than that reported by PHOBOS [50] at the same energy. PHENIX results are not included because they were reported for broader centrality bins. WA97 results are also omitted because they were measured at higher transverse momenta.

Comparative studies are a necessary part of searches for nontrivial structures in the excitation function that might arise from a possible phase transition [3]. The radius parameter $R_{\rm side}$ has the most direct correlation with the source geometry, whereas $R_{\rm out}$ encodes both geometry and time-scale information. Experimental results show that $R_{\rm side}$ decreases at AGS energies and then displays a modest rise with collision energy from SPS to RHIC. $R_{\rm long}$ increases with collision energy after an initial decrease at the lower AGS energies. For $R_{\rm out}$ the changes are very small.

Hydrodynamic model calculations [3,4] predict an enhancement in the ratio of $R_{\rm out}/R_{\rm side}$ with increasing beam energy. The experimental results show no such behavior. The measured ratios are better reproduced by the AMPT (multiphase transport) model [58], however the individual predicted radii have a steeper decrease compared to the experimental data [8]. An alternative model using a relativistic quantum mechanical treatment of opacity and the refractive index is capable of reproducing the observed results [59] but strongly depends on the assumed initial conditions and neglects the time dependence of the corresponding optical potential. Hydrodynamic calculations [60] including viscosity offer another possible explanation for the above deviation between the data and model calculations as recently shown in Ref. [61]. According to recent hydrodynamic calculations, the femtoscopic radii can be described either by using the initial Gaussian density profile [62] or by including the combination of several effects including prethermal acceleration, a stiffer equation of state, and additional viscous corrections [63].

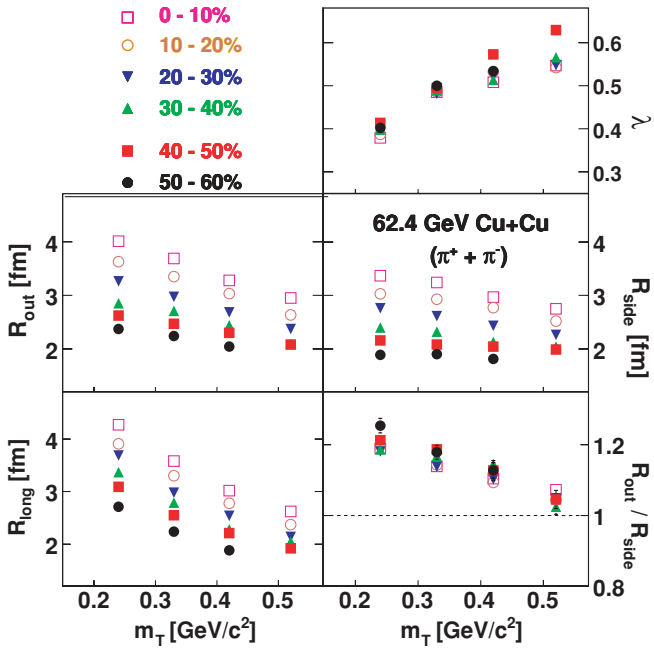

FIG. 4. (Color online) Femtoscopic parameters vs. m_T for six centralities for Cu + Cu collisions at $\sqrt{s_{NN}} = 62.4$ GeV. Only statistical errors are shown. The estimated systematic errors are less than 10% for $R_{\rm out}$, $R_{\rm side}$, $R_{\rm long}$, λ in all centrality and k_T bins.

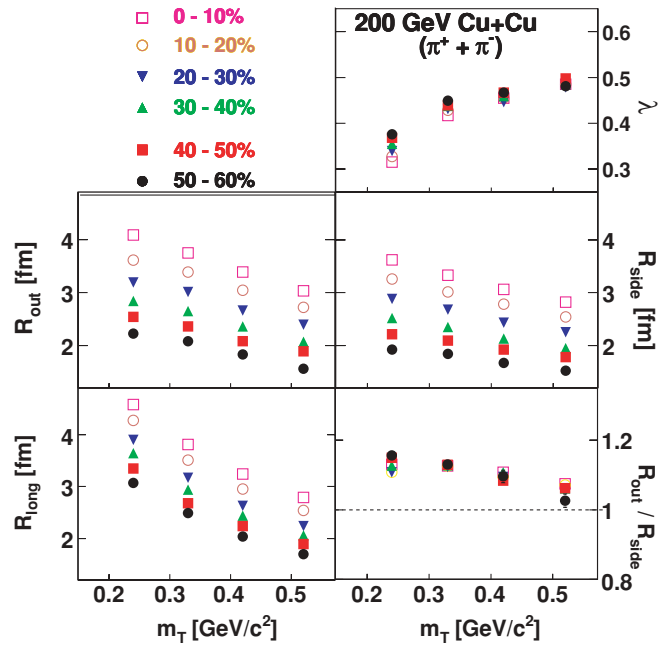

FIG. 5. (Color online) Femtoscopic parameters vs. m_T for six centralities for Cu + Cu collisions at $\sqrt{s_{NN}} = 200$ GeV. Only statistical errors are shown. The estimated systematic errors are less than 10% for $R_{\rm out}$, $R_{\rm side}$, $R_{\rm long}$, λ in all centrality and k_T bins.

Other recent studies with a granular source model [64] also obtain a better description of the experimental measurements of pion femtoscopic radii.

C. Cu + Cu collisions at $\sqrt{s_{NN}} = 62.4$ and 200 GeV

The correlation functions are similarly constructed for Cu + Cu collisions at $\sqrt{s_{NN}} = 62.4$ GeV and 200 GeV. The extracted femtoscopic radii, $R_{\rm out}$, $R_{\rm side}$, and $R_{\rm long}$, along with the λ parameter and the ratio $R_{\rm out}/R_{\rm side}$ are presented in Figs. 4 and 5 for the 62.4 and 200 GeV data, respectively. The results are presented for six different centralities and four m_T bins. The highest k_T bin [450–600] MeV/c of the most peripheral centrality (50–60%) in Cu + Cu collisions at $\sqrt{s_{NN}} =$ 62.4 GeV is omitted due to inadequate statistics for decomposition with the Bertsch-Pratt parametrization. For both collision energies the three femtoscopic radii increase with increasing centrality, whereas the λ parameter shows no centrality dependence. The m_T dependences of the femtoscopic radii are similar to that for Au + Au collisions. The $R_{\rm out}/R_{\rm side}$ ratios exhibit no clear centrality dependences for either energy.

D. Comparison of femtoscopic radii for Cu + Cu and Au + Au collisions

In Fig. 6 the femtoscopic source parameters λ, $R_{\rm out}$, $R_{\rm side}$, $R_{\rm long}$ and the ratio $R_{\rm out}/R_{\rm side}$ for central (0–5%) Au + Au collisions at $\sqrt{s_{NN}} = 200$ GeV [17] are compared with central (0–10%) Cu + Cu collisions at same beam energy. As expected, the femtoscopic radii for Cu + Cu collisions are smaller than for Au + Au collisions at the same beam energy.

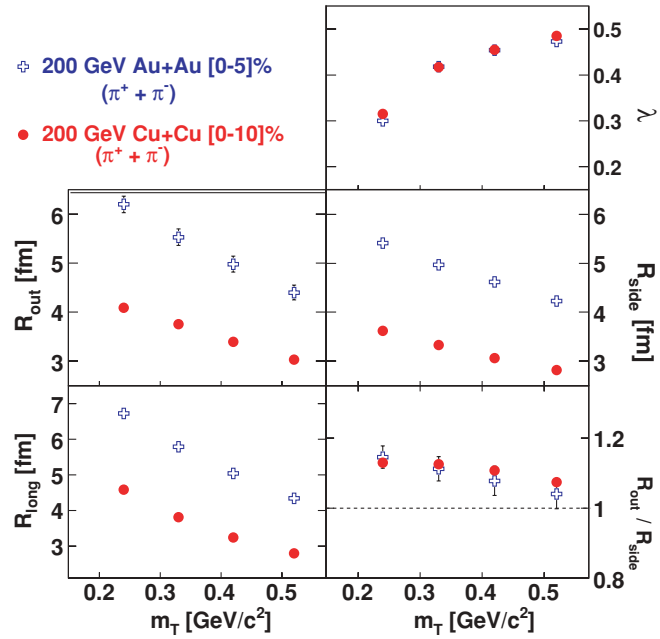

FIG. 6. (Color online) The comparison of system size dependence in femtoscopic measurements of STAR Au + Au and Cu + Cu collisions at $\sqrt{s_{NN}} = 200$ GeV. Only statistical errors are shown for Cu + Cu collisions at $\sqrt{s_{NN}} = 200$ GeV. The estimated systematic errors for Cu + Cu collisions at $\sqrt{s_{NN}} =$ 200 GeV are less than 10% for $R_{\rm out}$, $R_{\rm side}$, $R_{\rm long}$, λ in 0–10% most central events and k_T bins. The Au + Au results are from Ref. [17].

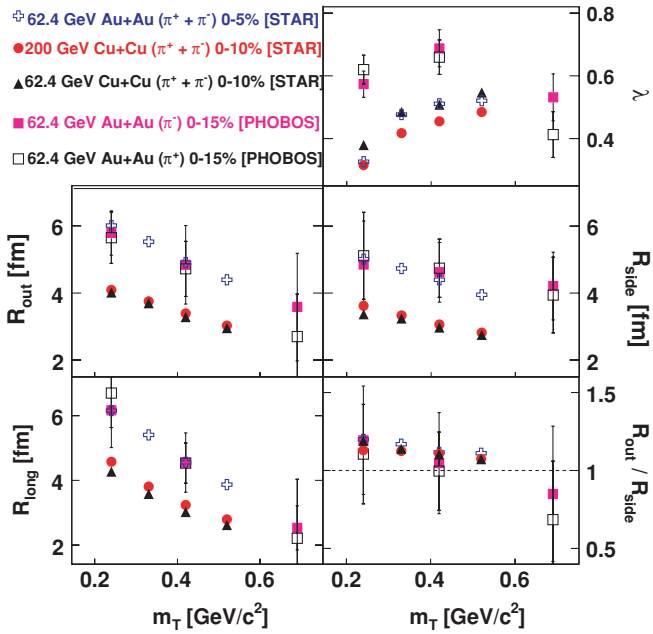

FIG. 7. (Color online) The comparison of femtoscopic measurements of STAR Cu + Cu collisions at $\sqrt{s_{NN}} = 200$ and 62.4 GeV and Au + Au collisions at $\sqrt{s_{NN}} = 62.4$ GeV. Only statistical errors are shown for STAR results. The estimated systematic errors for STAR results are less than 10% for $R_{\rm out}$, $R_{\rm side}$, $R_{\rm long}$, λ in all centrality and k_T bins. The PHOBOS results [50] for positive and negative pions in Au + Au collisions at $\sqrt{s_{NN}} = 62.4$ GeV are compared with STAR results.

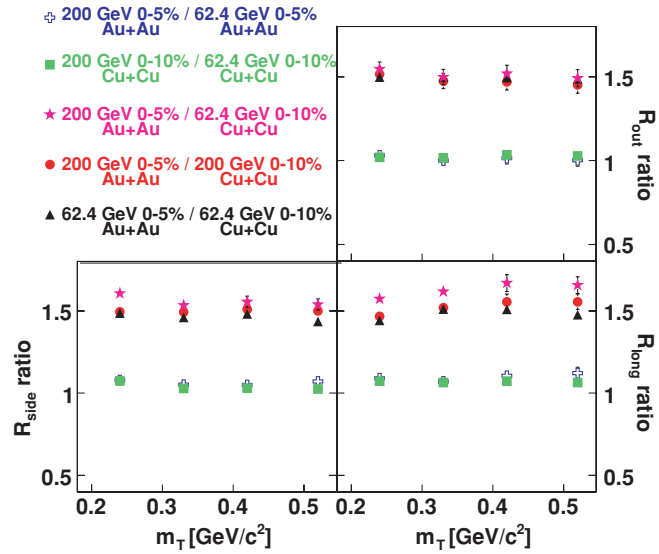

FIG. 8. (Color online) Ratios of femtoscopic radii at top centralities for Au + Au and Cu + Cu collisions at $\sqrt{s_{NN}} = 200$ and 62.4 GeV vs. m_T. Only statistical errors are shown for Au + Au collisions at $\sqrt{s_{NN}} = 62.4$ GeV and Cu + Cu collisions at $\sqrt{s_{NN}} = 62.4$ and 200 GeV. The estimated systematic errors for Au + Au collisions at $\sqrt{s_{NN}} = 62.4$ GeV and Cu + Cu collisions at $\sqrt{s_{NN}} = 62.4$ and 200 GeV are less than 10% for $R_{\rm out}$, $R_{\rm side}$, $R_{\rm long}$ in all centrality and k_T bins. The 200 GeV results are from Ref. [17].

It is interesting that the values of the ratio $R_{\rm out}/R_{\rm side}$ for the two systems are similar.

In Fig. 7 we extend the comparison of femtoscopic source parameters to include central (0–5%) Au + Au collisions at $\sqrt{s_{NN}} = 62.4$ GeV, central (0–10%) Cu + Cu collisions at $\sqrt{s_{NN}} = 62.4$ and 200 GeV, and central (0–15%) $\pi^+\pi^+$ and $\pi^-\pi^-$ correlations from Au + Au collisions at 62.4 GeV from the PHOBOS experiment [50]. The femtoscopic radii for Cu + Cu collisions at $\sqrt{s_{NN}} = 62.4$ GeV are smaller than those for Au + Au collisions at the same beam energy. The femtoscopic radii for Cu + Cu central collisions are similar for both energies. The variation of the $R_{\rm out}/R_{\rm side}$ ratio with m_T is similar for the Au + Au and Cu + Cu collision data.

In Fig. 8 we present the m_T dependences of the ratios of femtoscopic radii for the most-central Au + Au and Cu + Cu collisions at $\sqrt{s_{NN}} = 200$ and 62.4 GeV. Ratios for the same colliding ion systems are close to unity, whereas ratios of radii for Au + Au to Cu + Cu collisions are ∼1.5. Although the individual radii decrease significantly with increasing m_T the ratios in Fig. 8 show that the femtoscopic radii for Au + Au and Cu + Cu collisions at 62.4 and 200 GeV share a common m_T dependence. This result can be understood in terms of models [59,65] that use participant scaling to predict the femtoscopic radii in Cu + Cu collisions from the measured radii for Au + Au collisions at $\sqrt{s_{NN}} = 200$ GeV, assuming the radii are proportional to $A^{1/3}$, where A is the atomic mass number of the colliding nuclei.

E. Volume estimates and multiplicity scaling

Estimates of the pion freeze-out volume V_f in terms of the femtoscopic radii are provided by the following expressions:

$$V_f \propto R_{\rm side}^2 R_{\rm long} \tag{3a}$$

$$V_f \propto R_{\rm out} R_{\rm side} R_{\rm long}. \tag{3b}$$

However, the correlation lengths (femtoscopic radii) decrease with increasing m_T corresponding to an m_T-dependent region of homogeneity that, in expanding source models, is smaller than the true collision volume at freeze-out. The volume estimates [Eqs. (3a) and (3b)] are obtained from the lowest-m_T bin, corresponding to the k_T region from 150 to 250 MeV/c as discussed in Sec. II D.

The V_f measurements using Eq. (3a) as a function of $\sqrt{s_{NN}}$ are presented in Fig. 9 for Au + Au, Pb + Pb, and Pb + Au collisions at midrapidity and for the lowest-k_T bin defined above. The results show two distinct domains: first, at the AGS where the volume measure decreases, and second, in the SPS and RHIC energy regimes where a monotonic increase is observed.

A detailed description of this nontrivial behavior was suggested in Ref. [66] based on the hypothesis of constant mean-free-path length of pions at freeze-out. The explanation provided in Ref. [66] defines the pion mean-free-path length, λ_f, as:

$$\lambda_f = \frac{1}{\rho_f \sigma} = \frac{V_f}{N\sigma}, \tag{4}$$

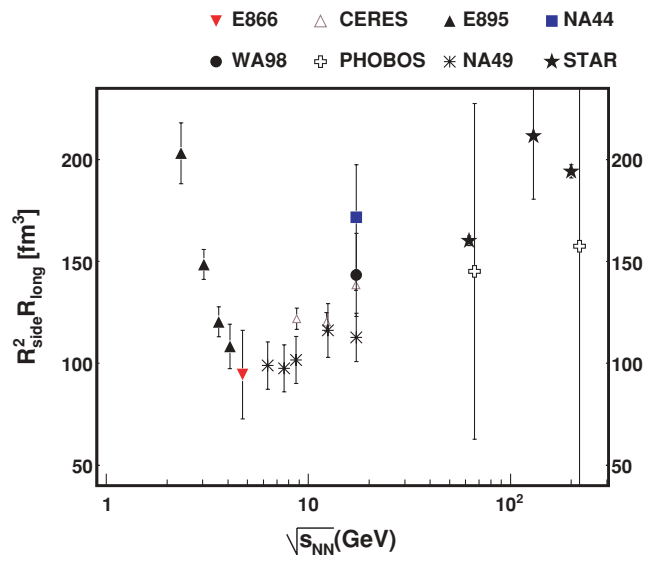

FIG. 9. (Color online) The energy dependence of the pion freeze-out volume for heavy-ion collision data from the AGS, SPS, and RHIC estimated using Eq. (3a). The references are given in the caption of Fig. 3. Only statistical errors are shown for Au + Au collisions at $\sqrt{s_{NN}} = 62.4$ GeV. The estimated systematic errors for Au + Au collisions at $\sqrt{s_{NN}} = 62.4$ GeV are less than 10% for $R_{\rm out}$, $R_{\rm side}$, $R_{\rm long}$ in all centrality and k_T bins.

where ρ_f is the freeze-out density and σ is the total cross section for pions to interact with the surrounding medium. The freeze-out density can be expressed as the number of particles N in the estimated freeze-out volume V_f, divided by V_f, resulting in the second expression in Eq. (4). The denominator, $N\sigma$, can be expanded as the sum of the pion-pion and pion-nucleon contributions. At AGS energies the pion-nucleon term dominates because the pion-nucleon cross section is larger than the pion-pion cross section. Also, the number of nucleons at these lower energies at midrapidity exceeds the number of pions. Hence, a decrease in the number of midrapidity nucleons leads to a decrease in the observed freeze-out volume (V_f) as a function of $\sqrt{s_{NN}}$. At SPS and RHIC energies the pion-pion term dominates the denominator in Eq. (4) due to copious pion production leading to an increase in the observed V_f.

Based on this interpretation we expect the volume estimates in the pion dominated RHIC regime to show a linear dependence on charged particle multiplicity. In Fig. 10 freeze-out volume estimates [using Eqs. (3a) and (3b)] are shown as a function of the number of participants (left panels) and charged particle multiplicity (right panels) for Au + Au collisions at $\sqrt{s_{NN}} = 62.4$ and 200 GeV. The predicted linear increase with charged particle multiplicity is observed. Estimated freeze-out volumes for Au + Au collisions at the same centralities

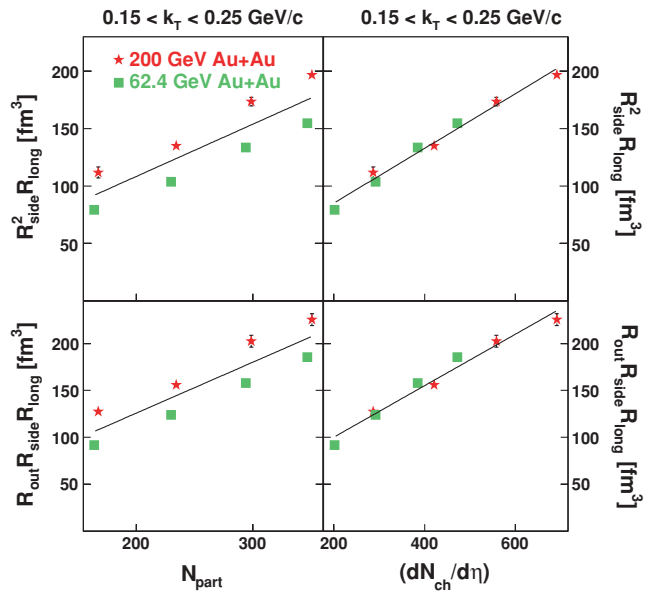

FIG. 10. (Color online) Pion freeze-out volume estimates as a function of number of participants and charged particle multiplicity density for Au + Au at $\sqrt{s_{NN}} = 200$ and 62.4 GeV. Only statistical errors are shown for Au + Au collisions at $\sqrt{s_{NN}} = 62.4$ GeV. The estimated systematic errors for Au + Au collisions at $\sqrt{s_{NN}} = 62.4$ GeV are less than 10% for $R_{\rm out}$, $R_{\rm side}$, $R_{\rm long}$ in all centrality and k_T bins. The 200 GeV Au + Au collision results are from Ref. [17]. The lines in each panel represent linear fits to the data.

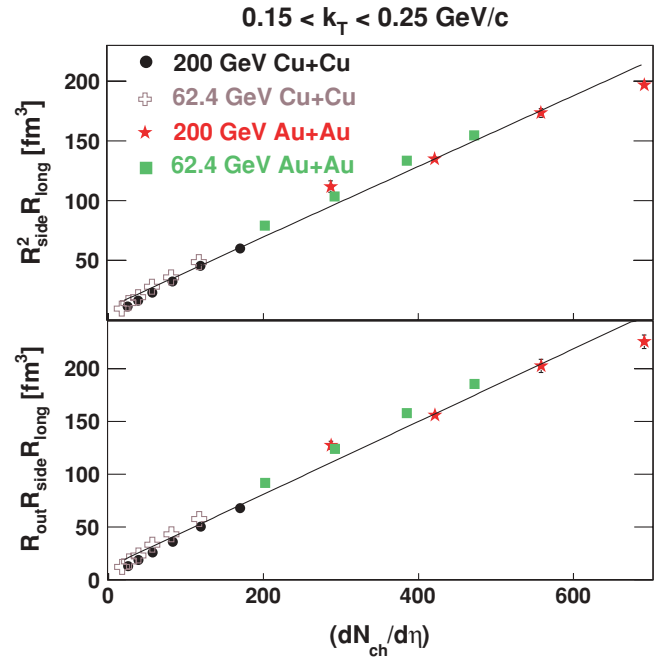

FIG. 11. (Color online) Pion freeze-out volume estimates as a function of charged particle multiplicity density for Au + Au and Cu + Cu collisions. Only statistical errors are shown for Au + Au collisions at $\sqrt{s_{NN}} = 62.4$ GeV and Cu + Cu collisions at $\sqrt{s_{NN}} = 62.4$ and 200 GeV. The estimated systematic errors for Au + Au collisions at $\sqrt{s_{NN}} = 62.4$ GeV and Cu + Cu collisions at $\sqrt{s_{NN}} = 62.4$ and 200 GeV are less than 10% for $R_{\rm out}$, $R_{\rm side}$, $R_{\rm long}$ in all centrality and k_T bins. The 200 GeV Au + Au collision results are from Ref. [17]. The lines in each panel represent linear fits to the data.

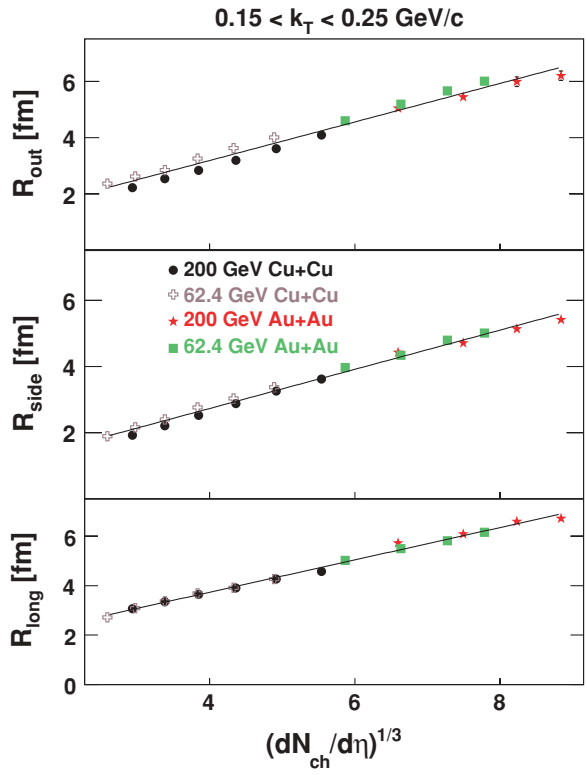

FIG. 12. (Color online) The pion source radii dependences on charged particle multiplicity density for Au + Au and Cu + Cu collisions. Only statistical errors are shown for Au + Au collisions at $\sqrt{s_{NN}} = 62.4$ GeV and Cu + Cu collisions at $\sqrt{s_{NN}} = 62.4$ and 200 GeV. The estimated systematic errors for Au + Au collisions at $\sqrt{s_{NN}} = 62.4$ GeV and Cu + Cu collisions at $\sqrt{s_{NN}} = 62.4$ and 200 GeV are less than 10% for $R_{\rm out}$, $R_{\rm side}$, $R_{\rm long}$ in all centrality and k_T bins. The 200 GeV Au + Au collision results are from Ref. [17]. The lines represent linear fits to the data.

increase with collision energy indicating that $N_{\rm part}$ is not a suitable scaling variable in this case. However, charged particle multiplicity provides better scaling properties.

Additional estimates of freeze-out volume dependences on charged particle multiplicity are presented in Fig. 11 for both the Au + Au and Cu + Cu results at $\sqrt{s_{NN}} = 62.4$ and 200 GeV. Both freeze-out volume estimates for the four collision systems show an approximate, common linear dependence on charged particle multiplicity. The linear dependences of femtoscopic radii on $(dN_{\rm ch}/d\eta)^{1/3}$ for Au + Au and Cu + Cu collisions at $\sqrt{s_{NN}} = 62.4$ and 200 GeV are shown in Fig. 12. The above common, linear dependences [8] are consistent with the assumption of a universal pion mean-free-path length at freeze-out [66].

V. SUMMARY AND CONCLUSIONS

We have presented systematic measurements of pion femtoscopy for Au + Au collisions at $\sqrt{s_{NN}} = 62.4$ GeV and Cu + Cu collisions at $\sqrt{s_{NN}} = 62.4$ and 200 GeV and compared these new results with our previous analysis of Au + Au collisions at $\sqrt{s_{NN}} = 200$ GeV [17]. For all the systems considered the three femtoscopic radii ($R_{\rm out}$, $R_{\rm side}$, and $R_{\rm long}$) increase with centrality, whereas the values of the λ parameter and ratio $R_{\rm out}/R_{\rm side}$ are approximately constant with centrality. The three femtoscopic radii decrease with increasing m_T, whereas the λ parameter increases with m_T. The increase of λ with m_T is attributed to decreasing contamination from pions produced from long-lived resonance decays at higher transverse momentum.

The decrease of femtoscopic radii with increasing m_T can be described by models with collective, transverse, and longitudinal expansion or flow. The ratios of femtoscopic radii at top centralities for different colliding systems (Au + Au and Cu + Cu) at $\sqrt{s_{NN}} = 62.4$ and 200 GeV show that the corresponding radii vary similarly with m_T.

The predicted rise of the ratio $R_{\rm out}/R_{\rm side}$ with collision energy due to a possible phase transition [3] is not observed for Au + Au and Cu + Cu collisions. The compilation of freeze-out volume estimates V_f as a function of collision energy $\sqrt{s_{NN}}$ [using Eq. (3a) along with the datasets presented in Fig. 3] shows two distinct domains: with increasing $\sqrt{s_{NN}}$, V_f decreases at the AGS but steadily increases throughout the SPS and RHIC energy regimes. At AGS energies the decreasing number of baryons at midrapidity leads to a decrease in the observed freeze-out volume (V_f) as a function of $\sqrt{s_{NN}}$. At higher beam energies from SPS to RHIC copious and increasing pion production causes the freeze-out volume to rise.

The dependences of the freeze-out volume estimate on number of participants and charged particle multiplicity are compared. Measurements for Au + Au collisions at the same centralities, but different energies yield different freeze-out volumes demonstrating that $N_{\rm part}$ is not a suitable scaling variable. The freeze-out volume estimates for all four collision systems presented here show a linear dependence on final charged particle multiplicity that is consistent with the hypothesis of a universal mean-free-path length at freeze-out.

For the systems studied here the multiplicity and k_T dependences of the femtoscopic radii are consistent with previously established trends at RHIC and at lower energies. The radii scale with the final-state collision multiplicity that, in a static model, is consistent with a hypothesized universal mean-free-path length at freeze-out. This and similar studies establish the baseline systematics against which to compare future femtoscopic studies at the Large Hadron Collider [67].

ACKNOWLEDGMENTS

We thank the RHIC Operations Group and RCF at BNL, and the NERSC Center at LBNL and the resources provided by the Open Science Grid consortium for their support. This work was supported in part by the Offices of NP and HEP within the US DOE Office of Science, the US NSF, the Sloan Foundation, the DFG cluster of excellence "Origin and Structure of the Universe," CNRS/IN2P3, RA, RPL, and EMN of France, STFC and EPSRC of the United Kingdom, FAPESP of Brazil, the Russian Ministry of Science and Technology, the NNSFC, CAS, MoST, and MoE of China, IRP and GA of the Czech

Republic, FOM of the Netherlands, DAE, DST, and CSIR of the Government of India and the Korea Science & Engineering Foundation. We thank Polish State Committee for Scientific Research, grant: N202 013 31/0489.

[1] J. C. Collins and M. J. Perry, Phys. Rev. Lett. **34**, 1353 (1975); E. V. Shuryak, Phys. Rep. **61**, 71 (1980); D. J. Gross, R. D. Pisarski, and L. G. Yaffe, Rev. Mod. Phys. **53**, 43 (1981); L. D. McLerran and B. Svetitsky, Phys. Lett. **B98**, 195 (1981).
[2] J. Adams *et al.* (STAR Collaboration), Nucl. Phys. **A757**, 102 (2005).
[3] D. H. Rischke and M. Gyulassy, Nucl. Phys. **A608**, 479 (1996).
[4] D. H. Rischke, Nucl. Phys. **A610**, 88c (1996).
[5] G. Goldhaber, S. Goldhaber, W. Y. Lee, and A. Pais, Phys. Rev. **120**, 300 (1960).
[6] R. Hanbury Brown and R. Q. Twiss, Phil. Mag. **45**, 663 (1954); Nature **178**, 1046 (1956).
[7] R. Lednicky, arXiv:nucl-th/0212089 [Presented at 32nd International Symposium on Multiparticle Dynamics (ISMD 2002), Alushta, Ukraine, 7–13 September 2002. Published in "Alushta 2002, Multiparticle dynamics", p. 21].
[8] M. A. Lisa, S. Pratt, R. Soltz, and U. Wiedemann, Annu. Rev. Nucl. Part. Sci. **55**, 357 (2005).
[9] G. I. Kopylov and M. I. Podgoretsky, Sov. J. Nucl. Phys. **15**, 219 (1972) [Yad. Fiz. **15**, 392 (1972)].
[10] U. W. Heinz and B. V. Jacak, Annu. Rev. Nucl. Part. Sci. **49**, 529 (1999).
[11] G. Bertsch, M. Gong, and M. Tohyama, Phys. Rev. C **37**, 1896 (1988).
[12] S. Pratt, Phys. Rev. D **33**, 1314 (1986).
[13] S. Chapman, P. Scotto, and U. W. Heinz, Phys. Rev. Lett. **74**, 4400 (1995).
[14] C. Adler *et al.* (STAR Collaboration), Phys. Rev. Lett. **87**, 082301 (2001).
[15] K. Adcox *et al.* (PHENIX Collaboration), Phys. Rev. Lett. **88**, 192302 (2002).
[16] S. S. Adler *et al.* (PHENIX Collaboration), Phys. Rev. Lett. **93**, 152302 (2004).
[17] J. Adams *et al.* (STAR Collaboration), Phys. Rev. C **71**, 044906 (2005).
[18] G. Baym, Acta Phys. Pol. B **29**, 1839 (1998).
[19] S. S. Padula, Braz. J. Phys. **35**, 70 (2005).
[20] E. V. Shuryak, Phys. Lett. **B44**, 387 (1973).
[21] L. D. McLerran, in *Physics and Astrophysics of Quark-Gluon Plasma*, edited by Bikash Sinha and Sibaji Raha (World Scientific, 1988), p. 16.
[22] U. W. Heinz, arXiv:nucl-th/9609029 [Presented in the International Summer School on Correlations and Clustering Phenomena in Subatomic Physics, Dronten, Netherlands, 5–16 August 1996. Published in "Dronten 1996, Correlations and clustering phenomena in subatomic physics", p. 137].
[23] U. A. Wiedemann and U. W. Heinz, Phys. Rep. **319**, 145 (1999).
[24] U. W. Heinz, Nucl. Phys. **A610**, 264c (1996).
[25] B. Tomasik and U. A. Wiedemann, arXiv:hep-ph/0210250 [Published in Quark Gluon Plasma 3, edited by R. C. Hwa and X. N. Wang, World Scientific, Singapore, 2003, p. 715].
[26] K. H. Ackermann *et al.* (STAR Collaboration), Nucl. Instrum. Methods A **499**, 624 (2003).
[27] K. H. Ackermann *et al.* (STAR Collaboration), Nucl. Phys. **A661**, 681 (1999).
[28] C. Adler, A. Denisov, E. Garcia, M. J. Murray, H. Strobele, and S. White, Nucl. Instrum. Methods A **470**, 488 (2001).
[29] J. Adams *et al.* (STAR Collaboration), Phys. Rev. C **73**, 034906 (2006).
[30] M. L. Miller, K. Reygers, S. J. Sanders, and P. Steinberg, Annu. Rev. Nucl. Part. Sci. **57**, 205 (2007).
[31] H. Bichsel, Nucl. Instrum. Methods A **562**, 154 (2006).
[32] B. I. Abelev *et al.* (STAR Collaboration), Phys. Rev. C **79**, 034909 (2009).
[33] M. I. Podgoretsky, Sov. J. Nucl. Phys. **37**, 272 (1983).
[34] P. Grassberger, Nucl. Phys. **B120**, 231 (1977).
[35] R. Lednicky and V. L. Lyuboshitz, Sov. J. Nucl. Phys. **35**, 770 (1982).
[36] M. Gyulassy, S. K. Kauffmann, and L. W. Wilson, Phys. Rev. C **20**, 2267 (1979).
[37] D. H. Boal, C. K. Gelbke, and B. K. Jennings, Rev. Mod. Phys. **62**, 553 (1990).
[38] Yu. Sinyukov, R. Lednicky, S. V. Akkelin, J. Pluta, and B. Erazmus, Phys. Lett. **B432**, 248 (1998).
[39] M. A. Lisa and S. Pratt, arXiv:0811.1352 [nucl-ex].
[40] P. F. Kolb and U. W. Heinz, arXiv:nucl-th/0305084 [Published in Quark Gluon Plasma 3, edited by R. C. Hwa and X. N. Wang, World Scientific, Singapore, 2003, p. 634].
[41] F. Retiere and M. A. Lisa, Phys. Rev. C **70**, 044907 (2004).
[42] T. Hirano and K. Tsuda, Nucl. Phys. **A715**, 821 (2003).
[43] B. Tomasik, U. A. Wiedemann, and U. W. Heinz, Nucl. Phys. **A663**, 753 (2000).
[44] U. A. Wiedemann, P. Scotto, and U. W. Heinz, Phys. Rev. C **53**, 918 (1996).
[45] U. A. Wiedemann, Phys. Rev. C **57**, 266 (1998).
[46] S. Pratt, Phys. Rev. Lett. **53**, 1219 (1984).
[47] B. R. Schlei and N. Xu, Phys. Rev. C **54**, R2155 (1996).
[48] B. R. Schlei, U. Ornik, M. Plumer, and R. M. Weiner, Phys. Lett. **B293**, 275 (1992).
[49] A. N. Makhlin and Y. M. Sinyukov, Z. Phys. C **39**, 69 (1988).
[50] B. B. Back *et al.* (PHOBOS Collaboration), Phys. Rev. C **73**, 031901 (2006).
[51] L. Ahle *et al.* (E802 Collaboration), Phys. Rev. C **66**, 054906 (2002).
[52] D. Adamova *et al.* (CERES Collaboration), Nucl. Phys. **A714**, 124 (2003).
[53] M. A. Lisa *et al.* (E895 Collaboration), Phys. Rev. Lett. **84**, 2798 (2000).
[54] I. G. Bearden *et al.* (NA44 Collaboration), Phys. Rev. C **58**, 1656 (1998).
[55] C. Alt *et al.* (NA49 Collaboration), Phys. Rev. C **77**, 064908 (2008).
[56] R. A. Soltz *et al.* (E866 Collaboration), Nucl. Phys. **A661**, 439 (1999).
[57] M. M. Aggarwal *et al.* (WA98 Collaboration), Phys. Rev. C **67**, 014906 (2003).
[58] Z. W. Lin, C. M. Ko, and S. Pal, Phys. Rev. Lett. **89**, 152301 (2002).
[59] J. G. Cramer, G. A. Miller, J. M. S. Wu, and J. H. S. Yoon, Phys. Rev. Lett. **94**, 102302 (2005).
[60] D. Teaney, Phys. Rev. C **68**, 034913 (2003).

[61] P. Romatschke, Eur. Phys. J. C **52**, 203 (2007).
[62] W. Florkowski, W. Broniowski, M. Chojnacki, and A. Kisiel, arXiv:0811.3761 [nucl-th].
[63] S. Pratt, Phys. Rev. Lett. **102**, 232301 (2009).
[64] W. N. Zhang and C. Y. Wong, arXiv:hep-ph/0702120.
[65] G. A. Miller and J. G. Cramer, J. Phys. G **34**, 703 (2007).
[66] D. Adamova *et al.* (CERES Collaboration), Phys. Rev. Lett. **90**, 022301 (2003).
[67] B. Alessandro *et al.* (ALICE Collaboration), J. Phys. G **32**, 1295 (2006).